EHD Study of the Corona Wind between Wire and Plate Electrodes

Akira Yabe,* Yasuo Mori,† and Kunio Hijikata‡
Tokyo Institute of Technology, Tokyo, Japan

The corona wind, with a velocity of several meters per second, is caused by applying high electric tension to bring about corona discharge in gases. In this paper the corona wind is experimentally and theoretically analyzed from an electrohydrodynamical (EHD) standpoint. Experiments have been performed mainly in nitrogen by a two-dimensional electrode arrangement of a fine wire anode and a plate cathode. The voltage-current characteristics of an electrostatic probe indicate that positive ions predominate in the whole space except in an extremely narrow region close to the wire. A theoretical analysis has been conducted based on the model that positive ions produced by ionization near the wire electrode move toward the plate, introducing the bulk convective motion of neutral molecules as the result of collisions of ions and neutral molecules. The electric potential distribution in the space and pressure distribution on the plate calculated numerically agree well with the experimental data. Consequently, it is made clear that the corona wind is caused by the Coulomb force exerted on ions and collisions of ions and neutral molecules of gas.

Nomenclature

b = mobility, $m^2/kV \cdot s$
C = constant, $\mu A/kV^2 \cdot m$
D = distance between wire and plate electrodes, m
d = diameter of wire electrode, m
E = electric field, kV/m
e = elementary electric charge, C
I = discharge current per unit wire length, $\mu A/m$
J = current density, $\mu A/m^2$
J_{wo} = maximum current density on plate electrode, $\mu A/m^2$
J_w = current density on plate electrode, $\mu A/m^2$
n = number density of positive ions, m^{-3}
n_0 = characteristic charge number density $= DJ_{wo}/eb\phi_o$, m^{-3}
Re_E = EHD Reynolds number $= U_E \cdot D/\nu$
U_E = EHD characteristic velocity $= \sqrt{DJ_{wo}/\rho b}$, m/s
u = velocity of neutral fluid (x component), m/s
v = velocity of neutral fluid (y component), m/s
x,y,z = rectangular coordinates (Fig. 1), m
Δx = mesh size of numerical calculation for x coordinate
Y = $D^3 J_{wo}/\epsilon b\phi_0^2$
Δy = mesh size of numerical calculation for y coordinate
ϵ = permeability, F/m
ν = kinematic viscosity, m^2/s
ξ,η = bipolar coordinates
ρ = neutral gas density, kg/m^3
ϕ = electric potential, kV
ϕ_0 = electric potential between wire and plate, kV
ψ = stream function, m^2/s
ω = vorticity, s^{-1}
= nondimensional quantity

Subscripts

x = x component
y = y component

I. Introduction

THE flow of neutral molecules, with velocities of several meters per second, can occur in a gas by applying high electric tension between a needle or wire electrode and a plate electrode. This flow has been known for some time[1,2] and has been often called the corona wind, the ionic wind, or the electric wind. Occurring in a field where convective heat transfer or mass transfer is required, this wind makes transfer coefficients increase substantially.[3,4] As a practical application of this effect, the cooling of bodies in gases called the electrostatic cooling, has been studied.[5,6] The mechanism by which ions give their momentum to neutral molecules is considered[7] to be similar to that in EHD power generation, and a fundamental study of the corona wind is also important for the EHD power generation. However, there are several simple explanations[1] of the mechanism and one-dimensional analyses,[2] which treat the average flow.

The purpose of this paper is to make an EHD analysis of the corona wind. The electric and fluid fields are analyzed to make a quantitative comparison of the theory with experiments from the EHD standpoint. The most adequate arrangement of the electrodes to make a fundamental investigation based on the standpoint just mentioned is a two-dimensional one consisting of the downward facing plate cathode and a wire anode under the plate.

Received Oct. 4, 1977; revision received Dec. 6, 1977.

Index categories: Hydrodynamics; Plasma Dynamics and MHD.

*Graduate Student, Department of Physical Engineering.
†Professor, Department of Physical Engineering.
‡Research Associate, Department of Physical Engineering.

II. Experiment

A. Experimental Apparatus

The outline of the experimental setup is shown in Fig. 1a. A platinum fine wire electrode of 40-μm diam. was stretched horizontally as an anode. A horizontal copper flat plate electrode 0.1-m long and 0.1-m wide facing downward was fixed over the wire. The two-dimensional nonuniform electric field was realized by applying high electric tension between the electrodes. The length of the wire electrode was 0.12 m and covered with electrically insulating paste over the 0.01-m length from both ends in order to minimize the influence of the end supporting parts. As an electrostatic Langmuir probe, a nickel wire of 3.0×10^{-4}-m diam. was used and covered with the tapered glass tube leaving the active part. Considering that the current of the probe was proportional to the active length of the probe, the length was taken as 2.0×10^{-2} m. To change the gas and its pressure around the wire and plate electrodes, a closed chamber of plastic plates was used, which contained the plate electrode at the top of the chamber and the wire electrode in it. When the gas was changed, the chamber was evacuated down to 15 Pa and then dried gas was introduced into it. The static pressure on the plate electrode

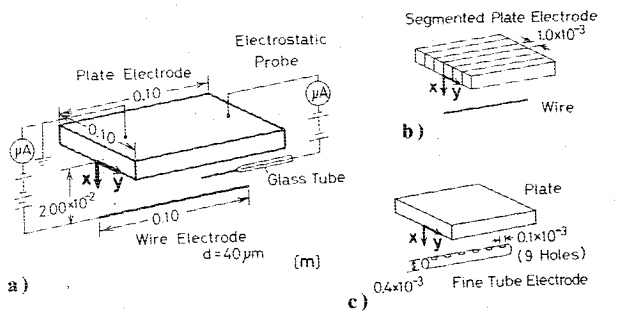

Fig. 1 Experimental setup: a) standard experimental arrangement, b) segmented plate electrode arrangement for measuring current density distribution on the plate, c) fine tube electrode arrangement for measuring the pressure near the fine tube.

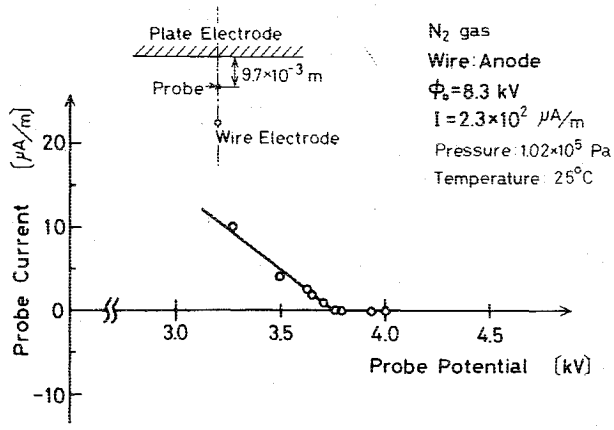

Fig. 2 Voltage-current relation of the electrostatic probe.

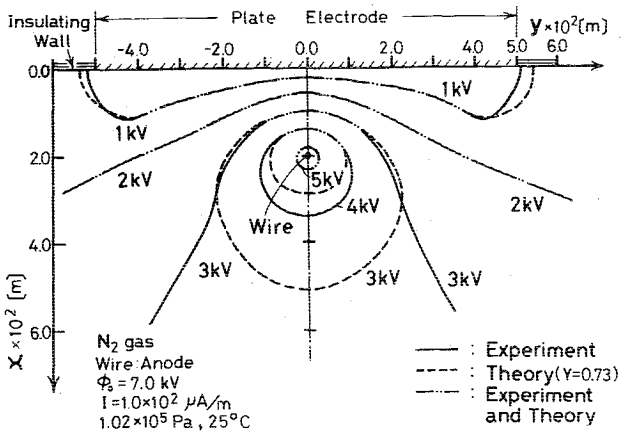

Fig. 3 Measured and calculated space potential distribution.

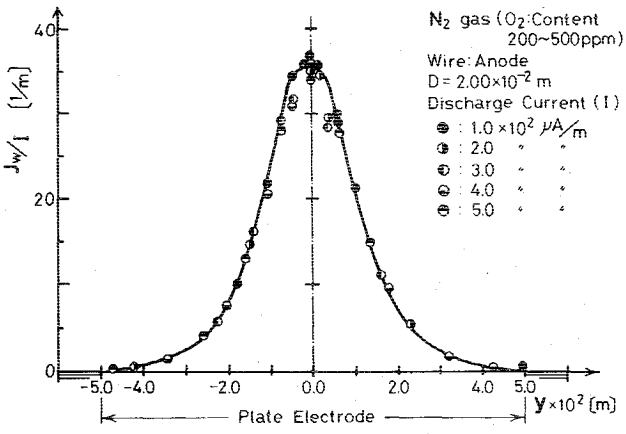

Fig. 4 Current density distribution on the plate electrode.

was measured as the pressure difference from the static pressure at the bottom of the chamber by using a Chattock gage with the accuracy of 0.1 Pa. The diameter of static pressure holes on the plate is 0.6×10^{-3} m. All experiments were carried on at room temperature and pressure 1.0×10^{5} Pa. As a power source of high electric tension, an optically controlled power source of fluctuation of below 1% was adopted. The power source for the electrostatic probe was also made on the same principle. The distance between the wire and plate electrodes was taken to be 2.0×10^{-2} m in order that a two-dimensional electric field could be realized with good accuracy. To measure the current density distribution on the plate electrode, another segmented plate electrode consisting of many slender copper plates 1.0×10^{-3} m thick and thin teflon insulation sheets 0.1×10^{-3} m thick was used instead of the plate electrode as shown in Fig. 1b.

B. Experimental Results of Electric Field

When nitrogen was introduced in the chamber and the electric potential between the wire anode and the grounded plate cathode was increased gradually, no current was observed up to a specific potential and above this potential the current began to increase due to the corona glow discharge. The observed voltage-current relation in the corona glow discharge region agreed well with the empirical formula[8] known so far. The relation is given by $I=C\phi_0\ (\phi_0-\phi_s)$ where I is the discharge current per unit wire length; ϕ_0 is the applied electric potential between the wire and the plate; ϕ_s is the corona discharge starting potential of 4 kV for the electrodes distance of $D=2.0\times10^{-2}$ m in our experiment; and C is the constant value of 5.5 μA/kV$^2\cdot$m. For air C is found to be 5.5 μA/kV$^2\cdot$m. The phenomenon of the corona discharge is changed as the current is increased further. In our experiment the corona glow discharge of an extremely narrow lightening zone close to the wire electrode was observed.

On the basis that the corona glow discharge was realized, the electrostatic probe was set in between the electrodes and the positive potential was applied to the probe to measure the voltage-current relation of the probe, an example of which is shown in Fig. 2. When the probe potential exceeds a specific potential, the probe current disappears, indicating that there is no electron current. The relations similar to that shown in Fig. 2 were observed by traversing the probe through the whole space except the extremely narrow region within 0.5×10^{-3}-m radius away from the wire. Therefore, it is experimentally confirmed that there are few electrons in the whole space except in the extremely narrow region close to the wire, and that there are only positive ions and neutral molecules in almost the entire field. Judging from the probe characteristics shown in Fig. 2, the lowest potential for no probe-current can be regarded as the space potential at the point. The space potential distributions obtained experimentally in nitrogen for the discharge current I of 1.0×10^{2} μA/m are shown by the solid line in Fig. 3. These potential distributions are different from those without ions and this fact will be discussed later in detail in connection with Fig. 9.

When the corona discharge was realized in nitrogen and the discharge current was in the region of 1.0×10^{2} μA/m $\sim 5.0\times10^{2}$ μA/m, the measured current density J_w on the segmented plate electrode divided by the total current I is plotted in Fig. 4. As is evident from the figure, the shape of the normalized current density distribution is independent of the total current. This shape is the same for air and independent of the wire diameter in the range of 40 μm-400 μm.

C. Experimental Results of Fluid Field

In the pressure measurement, the pressure at the bottom of the chamber was taken as the reference pressure because the

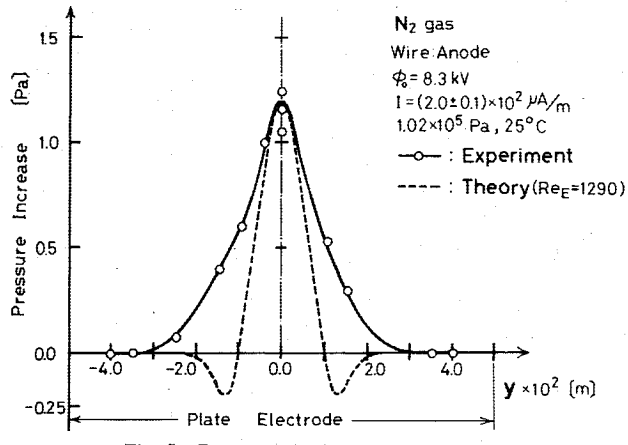

Fig. 5 Pressure distribution on the plate.

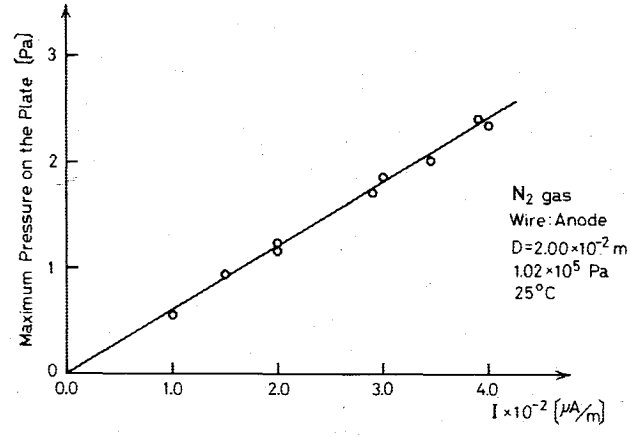

Fig. 6 Relations between the maximum pressure on the plate and the discharge current.

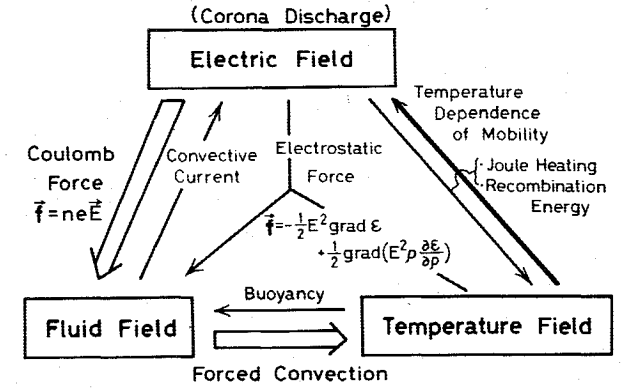

Fig. 7 Interactions among the electric, fluid, and temperature fields.

fluid velocity in the vicinity of the bottom was considered negligibly small. The measured pressure distribution on the plate in nitrogen for $I = 2.0 \times 10^2$ μA/m is shown in Fig. 5. Considering that the pressure increase at the center is caused by the dynamic pressure of the oncoming flow toward the plate, the velocity is calculated as 1.4 m/s.

In order to estimate the main velocity around the wire electrode, a fine tube was used as the electrode and for pressure measurement in its rear stagnation region. The tube was equipped with holes facing upward to the direction of the plate electrode as shown in Fig. 1c instead of the wire electrode. The pressure measured at the holes of the fine tube electrode was lower than the static pressure far away from the tube by 7 Pa for $I = 1.1 \times 10^2$ μA/m and by 13 Pa for $I = 2.2 \times 10^2$ μA/m. Therefore, assuming that the pressure difference corresponds to the dynamic pressure of the flow, the velocity around the fine tube was calculated as about 3 m/s for the former current. The two dimensionality of the fluid field was confirmed from the measurement of the pressure distribution on the plate.

The maximum pressure measured on the plate just over the wire as shown in Fig. 5 depends on the total current. The relationship between this maximum pressure and the discharge current obtained from experiments is shown in Fig. 6. The maximum pressure is linearly proportional to the total current. Therefore, assuming that this pressure corresponds to the total pressure of the stagnation flow, this figure indicates that the velocity of the corona wind increases with the square root of the current.

III. Theoretical Analysis

A. Analysis of Electric Field

Fundamental Equations

There are two types of forces which act on a fluid in an electrostatic field: the electrostatic force and the Coulomb force. Since the former is mainly affected by the temperature field, interactions among the electric, fluid, and temperature fields should be discussed to derive fundamental equations. The interactions among these fields are considered as shown in Fig. 7. Taking into account the experimental result described earlier and the fact that the electrostatic force is smaller by one order of magnitude than the Coulomb force in the whole region except the extremely narrow zone in the vicinity of the wire electrode, in case of the corona wind the major interactions are considered to be those shown in Fig. 7, denoted by broad arrows. In consideration of the results obtained from the probe experiments as shown in Fig. 2, in a model to simplify the fundamental equations it is assumed that 1) the corona glow discharge is restricted to an extremely narrow region near the wire; 2) positive ions, produced by ionization of the gas in the high electric field near the wire drift in the electric field under the Coulomb force to the plate electrode without recombination, and electrons are captured by the wire electrode; and 3) the ions give their momentum to neutral molecules by collisions creating the bulk flow of neutral molecules. Judging from the foregoing considerations, the electric field should be solved first and then the Coulomb force calculated from the results of the electric field analysis should be used to analyze the fluid field. Therefore in this chapter the analysis of electric field is performed and in the next chapter the fluid field is to be discussed.

From the preceding considerations, the following assumptions are made in simplifying the fundamental equations for the electric field:

1) A steady two-dimensional field is assumed. The analysis is confined to the constant discharge current without fluctuations by arcings.

2) There are only neutral molecules and positive ions in the field. It is confirmed by an order-of-magnitude estimation that electrons which exist in the ionizing region of the corona discharge have little effect on determining the electric potential distribution.

3) The diffusion effect of ions is much less than the drift effect due to the electric field and is neglected.

4) The drift velocity of ions is expressed as bE in terms of the ion mobility b and the electric field E, since ions collide with neutral molecules many times.

From these assumptions the mass conservation equation of positive ions and Poisson's equation are derived as follows:

Mass conservation equation of positive ions

$$(u+bE_x)\frac{\partial n}{\partial x}+(v+bE_y)\frac{\partial n}{\partial y}+nb\left(\frac{\partial E_x}{\partial x}+\frac{\partial E_y}{\partial y}\right)=0 \qquad (1)$$

Poisson's equation

$$\frac{\partial E_x}{\partial x}+\frac{\partial E_y}{\partial y}=\frac{ne}{\epsilon} \tag{2}$$

In Eq. (1) the convection terms are neglected compared with the conduction terms based on the experimental results showing that $u \ll bE_x$ and $v \ll bE_y$. Then these two equations are expressed by two unknowns of the electric potential ϕ and the charge number density n, and so the equations become closed and can be solved.

The bipolar coordinates ξ, η defined in Eq. (3) are adopted in place of the rectangular coordinates x, y, defined in Fig. 1 as $\xi=\text{const}$, indicate the equipotential line when there is no space charge.

$$x=\frac{D\cdot\sinh\xi}{\cosh\xi-\cos\eta},\quad y=\frac{D\cdot\sin\eta}{\cosh\xi-\cos\eta} \tag{3}$$

When the maximum electric current density on the plate is denoted by J_{wo} for an applied voltage ϕ_0 and the characteristic charge number density by which J_{wo} is realized for the average electric field ϕ_0/D, where D is the distance between the electrodes is denoted by n_0, then ϕ and n are made nondimensional by use of ϕ_0 and n_0, such as $\bar{\phi}=\phi/\phi_0$ and $\bar{n}=n/n_0$. By use of these nondimensional values Eqs. (1) and (2) are transformed as Eqs. (4) and (5), respectively.

$$\frac{\partial\bar{n}}{\partial\eta}\cdot\frac{\partial\bar{\phi}}{\partial\eta}+\frac{\partial\bar{n}}{\partial\xi}\cdot\frac{\partial\bar{\phi}}{\partial\xi}+\bar{n}\cdot\left(\frac{\partial^2\bar{\phi}}{\partial\eta^2}+\frac{\partial^2\bar{\phi}}{\partial\xi^2}\right)=0 \tag{4}$$

$$\frac{\partial^2\bar{\phi}}{\partial\eta^2}+\frac{\partial^2\bar{\phi}}{\partial\xi^2}=-Y\cdot\frac{\bar{n}}{(\cosh\xi-\cos\eta)^2} \tag{5}$$

where the parameter Y given by

$$Y=\frac{D^3J_{wo}}{\epsilon b\phi_0^2}\left(=\frac{n_0e/\epsilon\cdot D}{\phi_0/D}\right)$$

expresses the ratio of the electric field produced by space charge to the average electrostatic field along the vertical line above the wire. Y is a very important parameter in the analysis of the corona wind. As shown in Fig. 8, the adopted main boundary conditions are 1) the potentials at the wire and the plate electrode, 2) the symmetry of the potential distribution with respect to the x axis shown in Fig. 1, and 3) the measured current density distribution on the plate electrode.

Numerical Calculation and Results

Equation (4) was solved by a backward difference method from the plate to the wire, and Poisson's equation was solved by a block relaxation method.[9] Both equations were solved iteratively by turns until convergence was gained. The convergence criterion was that the maximum ratio of the difference of ϕ in consecutive iteration to ϕ itself became less than 1×10^{-5}.

The calculated electric potential distribution to be compared with the corresponding experimental result is shown in Fig. 3 by the broken lines in case of $Y=0.734$. As to equipotential lines, the theoretical result agrees very well with the experiment in the region between the wire and the plate electrodes and has a little difference in the remaining domain. The discrepancy near the edges of the plate electrode is considered due to the large mesh size in the numerical calculation, and that below the wire is due to the inaccuracies of the numerical calculation and the experiment. The calculated electric potential distributions on the x axis, which are most important and play an essential role in the corona wind, are compared with the experimental results in Fig. 9 for $I=1.0\times10^2$ μA/m and $I=2.0\times10^2$ μA/m. There is a good agreement between them. In Fig. 9 the potential distribution of the electrostatic field without any electric charge is also shown by the chain line for the electric tension of 6.7 kV. As is evident from the figure, the ion space charges have a strong effect on the electrostatic field. So, it is not correct to use the electric potential without space charge for an analysis of corona discharge. The value of a positive ion mobility for nitrogen was obtained from the potential distributions for these two cases to be $b=0.11$ m^2/kV·s. This value is about 40% less than the value of $b=0.18$ m^2/kV·s which has been reported recently[10] by use of drift tube. The discrepancy between them might be because the nitrogen in our experiments contains vapor impurity[11] of several ppm and the electric field is not uniform as described earlier. The wall of the chamber in the experiments was made of transparent methylmethacrylate for the convenience of visualization, and the mobility in nitrogen was found to decrease to $b=0.10$ m^2/kV·s when the vapor level of the organic material was about 3×10^2 ppm. The impurity level was reduced down to below 1 ppm by continuously and slightly renewing the gas without introducing serious effect to the corona wind and the mobility then measured was $b=0.12$ m^2/kV·s. In Ref. 12, $b=0.14$ m^2/kV·s, which is close to our value, was reported but is considered to be deteriorated by the very small amount of impurity, because a very small amount of impurity would have a great effect on the value of mobility.

The mobility of positive ions in air was also measured, as it is important for the practical usage of the corona wind. By measuring the potential at the point 5×10^{-3} m under the plate along the symmetric axis, the parameter Y was decided and then the mobility was obtained. The experiments are well explained by setting the mobility of ions in air as $b=0.12$ m^2/kV·s. This value is well taken as the mobility of positive ions in air for a practical usage, although it is influenced a little by impurities. This value is close to the reported value $b=0.14$ m^2/kV·s.[12] The mobility measured by the same

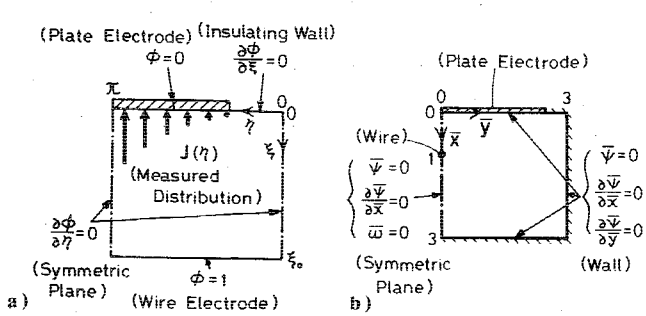

Fig. 8 Boundary conditions for numerical calculations: a) boundary conditions for the electric field, b) boundary conditions for the fluid field.

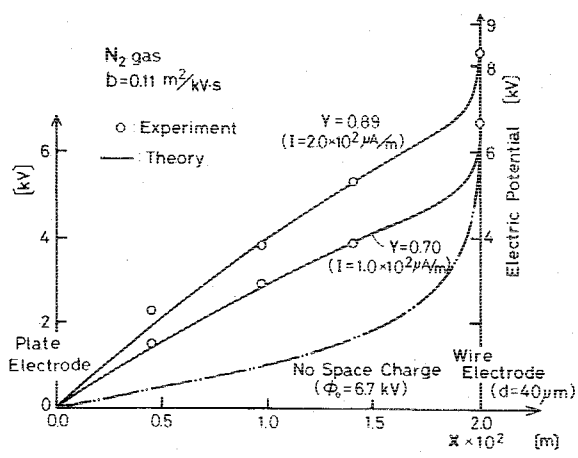

Fig. 9 Electric potential distributions along the x axis.

means in argon was 0.12 $m^2/kV \cdot s$ and that in CO_2 was 0.06 $m^2/kV \cdot s$.

B. Analysis of Fluid Field

Fundamental Equations

The fluid field is analyzed by making use of the distribution of the Coulomb force obtained by the numerical calculation of the electric field. The following two assumptions are made in the analysis:

1) The flow is two dimensional, steady, viscous, and incompressible. The Coulomb force working on the fluid is not the potential force and makes the flow rotational.

2) The existence of the wire is neglected. The diameter of the wire and its Reynolds number are too small to give an influence to the flow pattern in the enclosure.

The Coulomb force working on ions is understood as the force working on neutral molecules by collisions between ions and neutral molecules, and, thus, the Coulomb force neE enters in the momentum conservation equations of the fluid in the x and y components as the external force term. The conservation equation of vorticity is derived by eliminating the pressure terms from these momentum equations. The vorticity is defined as $\omega = (\partial v/\partial x) - (\partial u/\partial y)$. The velocity components u, v in the x, y directions are given as $u = (\partial\psi/\partial y)$, $v = -(\partial\psi/\partial x)$, respectively, by use of the stream function ψ. To express the vorticity equation in a nondimensional form the following nondimensional quantities are adopted:

$$\bar{x} = \frac{x}{D}, \quad \bar{y} = \frac{y}{D}, \quad \bar{n} = \frac{n}{n_0}, \quad \bar{\phi} = \frac{\phi}{\phi_0} \qquad \bar{\omega} = \frac{D}{U_E}\omega, \quad \bar{\psi} = \frac{\psi}{U_E \cdot D}$$

then the vorticity equation is given by

$$\frac{\partial\bar{\psi}}{\partial\bar{y}} \cdot \frac{\partial\bar{\omega}}{\partial\bar{x}} - \frac{\partial\bar{\psi}}{\partial\bar{x}} \cdot \frac{\partial\bar{\omega}}{\partial\bar{y}} = \left\{ \frac{\partial\bar{n}}{\partial\bar{y}} \cdot \frac{\partial\bar{\phi}}{\partial\bar{x}} - \frac{\partial\bar{n}}{\partial\bar{x}} \frac{\partial\bar{\phi}}{\partial\bar{y}} \right\} + \frac{1}{Re_E} \cdot \left\{ \frac{\partial^2\bar{\omega}}{\partial\bar{x}^2} + \frac{\partial^2\bar{\omega}}{\partial\bar{y}^2} \right\} \tag{6}$$

The defining equation of vorticity is

$$\frac{\partial^2\bar{\psi}}{\partial\bar{x}^2} + \frac{\partial^2\bar{\psi}}{\partial\bar{y}^2} = -\bar{\omega} \tag{7}$$

The parameter Re_E in Eq. (6) is expressed as follows:

$$Re_E = \frac{D \cdot U_E}{\nu} = \frac{D \cdot \sqrt{en_0\phi_0/\rho}}{\nu} = \frac{D \cdot \sqrt{DJ_{wo}/\rho b}}{\nu}$$

As understood from this relation, Re_E is Reynolds number having the EHD velocity U_E as the characteristic velocity and is now called EHD Reynolds number. U_E is the characteristic velocity of neutral molecules, which is obtained by setting the convection term of neutral molecules equal to the EHD force term.

Since n and ϕ in Eq. (6) have been already obtained by the numerical calculation of the electric field, Eqs. (6) and (7) have only two unknowns of ψ and ω. The boundary conditions for Eqs. (6) and (7) were taken as shown in Fig. 8b and numerical calculations were made only for the half right region.

Numerical Calculation and Results

Equation (6) is the second partial differential equation of an elliptic type. That was changed to a parabolic type by addition of the time differential term, and the unsteady equation thus obtained was numerically solved. The local time step Δt was chosen as large as possible under the condition of satisfying the stability criterion and depending on the local velocities u, v and the space meshes Δx, Δy as follows:

$$\Delta t = \frac{C}{\frac{2}{Re_E}\left\{\frac{1}{(\Delta x)^2} + \frac{1}{(\Delta y)^2}\right\} + \frac{|u|}{\Delta x} + \frac{|v|}{\Delta y}}$$

where C is taken as 0.9.

For the convection term of vorticity on the left-hand side of Eq. (6), the upwind differential method was used to improve the convergence of a numerical calculation for the larger value of Re_E. However, to increase the accuracy of numerical calculation near the surface of the plate, the convection term in Eq. (6) was changed from $[u(\partial\omega/\partial x)] + [v(\partial\omega/\partial y)]$ to $[\partial(u\omega)/\partial x] + [\partial(v\omega)/\partial y]$. Furthermore, as reported by Ozawa,[13] the upwind differential method has a disadvantage of poor accuracy because the magnitude of the first-order truncation error of the convection term would be about equal to or greater than the viscous term when Re_E is large. After obtaining the solution ω_A for a mesh size and the other solution ω_B for a half-mesh size, the value $\omega = 2 \times \omega_B - \omega_A$ was taken as the final value to minimize the first-order truncation error. If the following conditions are satisfied at every mesh point, the first-order difference scheme is improved to the second-order difference scheme in a way similar to how Keller et al.,[14] improved the second-order difference scheme to the fourth-order difference scheme:

$$u_A = u_B, \quad v_A = v_B, \quad \left(\frac{\partial^2\omega}{\partial x^2}\right)_A = \left(\frac{\partial^2\omega}{\partial x^2}\right)_B, \quad \left(\frac{\partial^2\omega}{\partial y^2}\right)_A = \left(\frac{\partial^2\omega}{\partial y^2}\right)_B$$

where A denotes the value for a mesh size and B denotes the one for a half-mesh size. Although there are some cases when u_A is not completely equal to u_B, considerable improvement of accuracy was attained by this method.

Equation (7) was the second partial differential equation of an elliptic type and was solved by a block relaxation method.[9] The two equations were solved iteratively by turns until the maximum value of the difference of ψ in consecutive iterations became less than 1×10^{-7}.

On the condition that the discharge current $I = 2.0 \times 10^2$ $\mu A/m$, the maximum current density $J_{wo} = 0.766 \times 10^4$ $\mu A/m^2$, the electric potential $\phi_0 = 8.3$ kV, the mobility of positive ions $b = 0.11$ $m^2/kV \cdot s$, the electrode distance $D = 2.0 \times 10^{-2}$ m, and that nitrogen is contained in the enclosure at room temperature and 1.02×10^5 Pa pressure, Eqs. (6) and (7) are numerically solved. EHD Reynolds number in this case is 1290. The stream function obtained from the numerical calculation for this case is shown in Fig. 10.

The vorticity is generated in the zone mainly between the electrodes and dissipated in the boundary layer along the plate

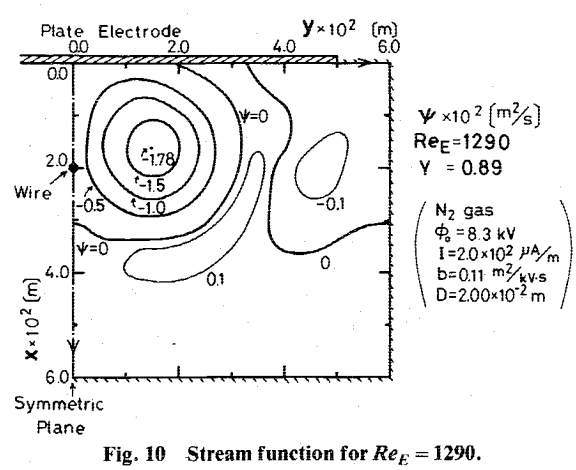

Fig. 10 Stream function for $Re_E = 1290$.

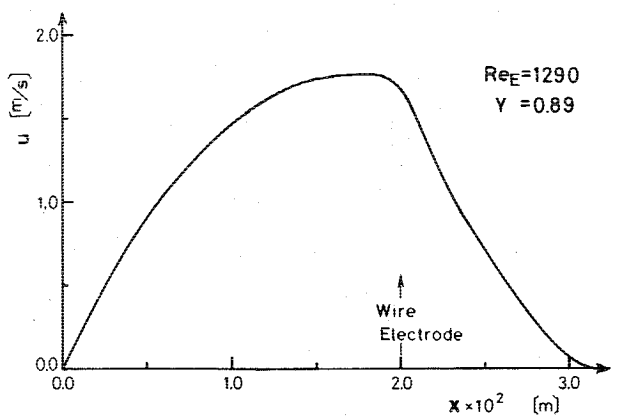

Fig. 11 Velocity distribution along the x axis.

electrode on account of the viscosity. As is obvious from the figure, the fluid field has the circulating flow. The region that has a velocity of more than 0.1 m/s is within the size of 3.5×10^{-2} m by 3.5×10^{-2} m, covering the region between the electrodes, and is small in the total space. The velocity distribution along the x axis calculated under the same condition as that for Fig. 10 is shown in Fig. 11. The velocity near the plate is proportional to the distance from the plate, showing the same performance as the potential flow close to a stagnant point, and reaches the maximum value of 1.8 m/s near the wire. Since the velocity of the oncoming flow toward the plate calculated from the measured maximum pressure on the plate shown in Fig. 5 is 1.4 m/s, the velocity near the wire is a little higher than that estimated from the measured pressure. As for the practical usage of the corona wind, this oncoming flow toward the plate can be applicable to cooling a body without using any fan or blower.

The calculated pressure distribution on the plate for this case is shown in Fig. 5 by the broken line. The static pressure at the bottom wall on the symmetric axis is taken as the reference pressure. As is evident from the figure, the maximum calculated value and the pressure distribution close to it agree very well with the measured values. However, in the region between 1.0×10^{-2} m and 2.5×10^{-2} m, which is near the separation point on the plate electrode obtained in the numerical calculation, the agreement between theory and experiment is not good, and the theoretical curve has the zone of pressure lower than the reference pressure. The reason for this discrepancy is considered to be due to the inaccuracy of the numerical calculation and the fluctuation of the separation point in experiments. The incompleteness of numerical calculation might push the separation point closer to the symmetric axis by overestimating the viscous term compared with the second-order centered difference approximation, since the truncation error of the convection term of Eq. (6) described earlier remains to a slightly extent, in spite of the improvement of the upwind differential method, due to the large value of Re_E. The three-dimensional fluctuation of the separation point would raise the lower pressure in the measurement. However, the coincidence of calculated and measured pressures near the symmetric axis is considered to support the model used in the analysis of the electric and fluid fields.

IV. Conclusion

To clarify the corona wind from an EHD standpoint, a corona wind produced by applying the high electric tension between a wire anode and a plate cathode, has been experimentally and theoretically investigated and the following conclusions have been obtained:

1) It is experimentally clarified that positive ions predominate over electrons in the whole space except in an extremely narrow region near the wire.

2) The numerically calculated electric potential distributions based on the model that only positive ions exist in the space are shown to agree very well with experimental results.

3) The two-dimensional steady incompressible viscous flow-field is calculated, taking into account the Coulomb force on ions. The pressure distribution on the plate obtained by numerical calculation agrees well with the experimental one near the maximum value. It is also shown that the fluid field is the circulating one.

4) It is quantitatively made clear that the corona wind is produced by the Coulomb force acting on ions.

Acknowledgment

Numerical calculations were carried out on the M-180 computer at the Tokyo Institute of Technology.

References

[1] Chattock, A. P., "On the Velocity and Mass of Ions in the Electric Wind in Air," *Philosophical Magazine*, Vol. 48, 1899, pp. 401-420.

[2] Robinson, M., "Movement of Air in the Electronic Wind of Corona Discharge," *AIEE Transactions*, Vol. 80, May 1961, pp. 143-150.

[3] Asakawa, Y., "Promotion and Retardation of Heat Transfer by Electric Fields," *Nature*, Vol. 261, May 1976, pp. 220-221.

[4] Chuang, T. H. and Velkoff, H. R., "Frost Formation in a Nonuniform Electric Field," *A.I.Ch.E. Symposium Series 113*, Vol. 67, 1971, pp. 10-18.

[5] Windishmann, H., "Investigation of Corona-Discharge Cooling of a Horizontal Plate under Free Convection," *A.I.Ch.E. Symposium Series 138*, Vol. 70, 1974, pp. 23-30.

[6] Velkoff, H. R. and Godfrey, R., "Low-Velocity Heat Transfer to a Flat Plate in the Presence of a Corona Discharge in Air," *ASME Publication*, 76-WA/HT-47, 1976.

[7] Kahn, B. and Gourdine, M. C., "Electrogasdynamic Power Generation," *AIAA Journal*, Vol. 2, Aug. 1964, pp. 1423-1427.

[8] Loeb, L. B., *Electrical Coronas*, 1st ed., Univ. Calif. Press, 1965, p. 45.

[9] Hijikata, K., Mori, Y., and Uchida, M., "Forced Convective Heat Transfer near the Trailing Edge of Flat Plate," *Proceedings of 5th International Heat-Transfer Conference*, Science Council of Japan, Tokyo, 1974, F.C.1.8, Pt. II, pp. 35-39.

[10] McDaniel, E. W. and Mason, E. A., *The Mobility and Diffusion of Ions in Gases*, Wiley, New York, 1973, p. 286.

[11] Loeb, L. B., *Basic Processes of Gaseous Electronics*, Univ. Calif. Press, 1955, p. 5.

[12] von Engel, A. and Steenbeck, M., *Elektrische Gasentladungen*, Vol. 1, Springer, Berlin, 1932, p. 182.

[13] Ozawa, S., "Numerical Studies of Steady Flow in a Two-Dimensional Square Cavity at High Reynolds Numbers," *Journal of the Physical Society of Japan*, Vol. 38, March 1975, pp. 889-895.

[14] Keller, H. B. and Cebeci, T., "Accurate Numerical Methods for Boundary-Layer Flows," *AIAA Journal*, Vol. 10, Sept. 1972, pp. 1193-1199.